Optical and physical properties of solgel-derived GeO_2:SiO_2 films in photonic applications

Charles K. F. Ho,[1] Rajni,[1] H. S. Djie,[1,2] Kantisara Pita,[1] Nam Quoc Ngo,[1,*] and T. Osipowicz[3]

[1]Photonics Research Centre, School of Electrical and Electronic Engineering, Nanyang Technological University, 50 Nanyang Avenue, Singapore 639798

[2]Department of Electrical and Computer Engineering, Lehigh University, Bethlehem, Pennsylvania, USA

[3]Centre of Ion Beam Applications, Department of Physics, National University of Singapore, Singapore 117542

*Corresponding author: eqnngo@ntu.edu.sg

Received 7 December 2006; accepted 13 February 2007;
posted 7 March 2007 (Doc. ID 77735); published 20 June 2007

The functionality of optical components relies heavily on the composition-dependent properties of germanosilicate materials, which include the refractive index, photosensitivity, and microstructural properties. Recent studies and parallel developments are presented of germanosilicate films with composition x of Ge content (i.e., xGeO$_2$:$(1 - x)$SiO$_2$) that were synthesized by the solgel process for various integrated photonic applications undertaken. The following novel aspects are discussed with respect to the effect of composition of the glassy films ($0.05 \le x \le 0.40$): determination of spectral optical properties, UV imprinting of optical waveguides with relatively large index change (Δn), and quantum-well intermixing enhancement observed in InGaAs(P)/InP quantum-well optical devices. The implications of the results are discussed. © 2007 Optical Society of America

OCIS codes: 160.6060, 130.3130, 130.0250, 130.5990, 310.6860, 230.5590.

1. Introduction

Ever since the deployment of optical fibers in the 1980s, the germanosilicate glass has been the material of choice for many devices operating within the telecommunication window. Soon after, photosensitivity in such glass was discovered, enabling the fabrication of devices such as fiber gratings, waveguide gratings, and recently the direct writing of optical devices [1,2]. Besides the ability to change the refractive index (RI) by either varying the composition of the germanosilicate or the dosage of UV exposure, the change in physical properties and microstructure can be exploited in some photonic applications. In this paper, we present our work on three aspects of germanosilicate films: spectral properties (viz., optical dispersion), UV photosensitivity leading to UV imprinting of optical waveguides, and porous germanosilicate films as an encapsulant layer for quantum-well intermixing (QWI).

With a higher electronic polarizability in GeO_2, its addition into a SiO_2 matrix is to raise the RI to achieve index guiding of near-infrared lightwaves. The relatively high RI of the core region affords stronger optical confinement, hence, reducing bend loss and device size [3–5]. Despite the number of prior studies of GeO_2:SiO_2 films [6–9] reports to date lack the spectroscopic details about the RI, which are valuable in the light of the foreseeable expansion in the telecommunication window (in the range of ~1.2 to 1.7 μm). Advances in metrology have enabled precise determinations of the optical constants of films by spectroscopic ellipsometry ($\le 10^{-3}$) [10]. Comprehensive characterization has been performed on the precise physical microstructure of the film samples, which allows an accurate determination of the dispersion (i.e., the spectral change of RI with wavelength) for different compositions [11]. The Sellmeier dispersion model was effectively used to describe the optical dispersion properties of the GeO_2:SiO_2 films for a range of wavelengths from 210 to 1700 nm.

The UV-induced RI change (photosensitivity) of the core layer presents an alternative technique with two attractive advantages in the fabrication of optical waveguide based devices. First, waveguiding devices

0003-6935/07/204397-10$15.00/0
© 2007 Optical Society of America

can be defined without the need to do lithography and etching where sidewall roughness adversely affects the performance of the waveguides. Secondly, post-fabrication adjustments of complex devices are possible to remedy for fabrication imperfections [12–15]. For large-scale device integration, one desirable attribute of direct-writing techniques is to achieve high permanent RI change (cf. RI contrast). Photosensitivity, in this context, refers to the photo-induced chemical modification of the inorganic glass, which results in a change in the RI, Δn. Although the exact mechanisms that cause such change in the RI are still the subject of debates at presence, many studies have shown that such photosensitivity is, in fact, associated with nonstoichiometric defects [16–20], which increase with the concentration of germanium [21–23]. Photosensitivity in optical fibers and, hence, fiber Bragg gratings have traditionally been restricted to values of $\Delta n \leq 10^{-4}$ [24,25]. On the other hand, planar optical waveguides provide a platform that has a substantially higher level of flexibility in terms of composition of the core. Recent works have reported achievements in the range of $\Delta n \leq 10^{-3}$ [24,26] fabricated by deposition methods such as vapour axial deposition and chemical vapor deposition (CVD) with additional UV-sensitization processes of hydrogen and thermal treatments. Recently, we demonstrated that an increase in RI up to 0.0098 has been achieved when our solgel derived germanosilicate films of approximately $\sim$200 nm in thickness were exposed to UV light. Such an increase in RI was attributed to the creation of an oxygen deficient center without employing any sensitization technique [27].

In another application dealing with photonic integration, we exploited the composition-dependent microstructural properties of the germanosilicate films. The technique of QWI [28] allows reliable and low-cost modifications of QW bandgap energy on the as-grown wafer. QWI has been found to be a more manufacturing-friendly process over the traditional growth–regrowth and selective-area growth process to achieve photonic integration because of its ability to selectively fine-tune the QW bandgap in different regions within the same epitaxial layer structure, through the interdiffusion between the QW and the adjacent barrier material [28,29]. The mechanisms that afford QWI involve the creation of disordering in the top barrier layer and subsequently the thermally activated interlayer diffusion of the created defects and constituents of the QW layers (i.e., Group III and V ions) leading to a change in the energy profile across the QW. Certainly, the QWs can tolerate only a suitable annealing temperature to promote the intermixing while retaining the crystalline quality. A high annealing temperature may cause the severe surface out-diffusion and dopant redistribution, which may contribute to the significant intrinsic waveguide loss due to free carrier absorption [29]. Compared with alternative techniques (e.g., laser-induced disordering, plasma-induced disordering, and impurity-induced disordering) [28] dielectric cap-induced disordering can be seen to be commercially attractive in large-scale production as it involves the deposition of a dielectric layer, which can be applied to large areas. In addition, device integration can be implemented economically by simple schemes involving area-selective bandgap modification [30,31]. The key to this process is the ability to tailor the dielectric properties to spatially control the interdiffusion rate in the QW. Hence the solgel process is expected to provide added values as a low-cost alternative of QWI techniques. While prior reports have shown the enhancement of QWI by the use of silica-based solgel caps on GaAs-based QWs with a very restrictive amount of doping of phorphorous [32,33] ($<$5 mol. %), our results [34] distinctly demonstrate the modification of excitonic emission in InP-based QWs using a highly doped solgel-silica cap. We discuss the effect of germanosilicate encapsulant layer (i.e., the dielectric cap) on the trimming of the bandgap energy of InGaAs(P)/InP QW laser structure.

2. Experimental Procedures

The raw materials of the solgel process incorporate precursors (tetraethoxysilane, 98% and germanium isopropoxide, 99.99%), which are readily soluble in common solvents. The details of the process are described in Fig. 1. Tetraethoxysilane (TEOS) was prehydrolyzed in a mixture (Sol-S) of ethanol and acidified (HCl) water of pH 1; the molar ratio of each component in the respective order was 1:4:2. Ge isopropoxide was diluted in anhydrous isopropanol at a molar ratio of 1:4 in a stock solution (Sol-G) in a N_2-purged glovebox (relative humidity $<$30%). An appropriate volume was later extracted from Sol-G and added to the Sol-S to become the Sol-SG for a desired composition of $x GeO_2:(1-x)SiO_2$ for $0.05 \leq x \leq 0.40$. After a period of ageing ($\sim$1–4 h) under rigorous mechanical agitation, the Sol-SG, was then spin coated on the desired substrate (silicon or III-V) depending on the intended applications. The dilution step was only used as needed to ensure that the solution remain clear during the ageing period. This spin-coating process was performed in a N_2-purged glovebox. The dried gel films were typically subjected to thermal treatment by a rapid thermal processor (RTP) for annealing periods for 20 s with a ramp rate of $\sim$25 °C/s or by an electric furnace with air ambient for annealing periods $>$10 min at temperature $>$1000 °C.

A. Thin Films for the Determination of the Spectral Properties

In the study of spectro-optical properties, thin films (thickness of $\sim$200 nm) of single coating were deposited at 1000 rpm on Si (100) substrates. The films were annealed in an electric furnace for 10 to 15 min at temperatures of 1000 °C to 1100 °C. The fabrication of planar waveguides followed closely the method proposed by Syms *et al.* [35,36]. Each coating was deposited at $\sim$2000 rpm. The dispersion properties of germanosilicate films were determined by the use of a variable angle spectroscopic ellipsometry (VASE) from J. A. Woollam, in a reflection mode at 60° and

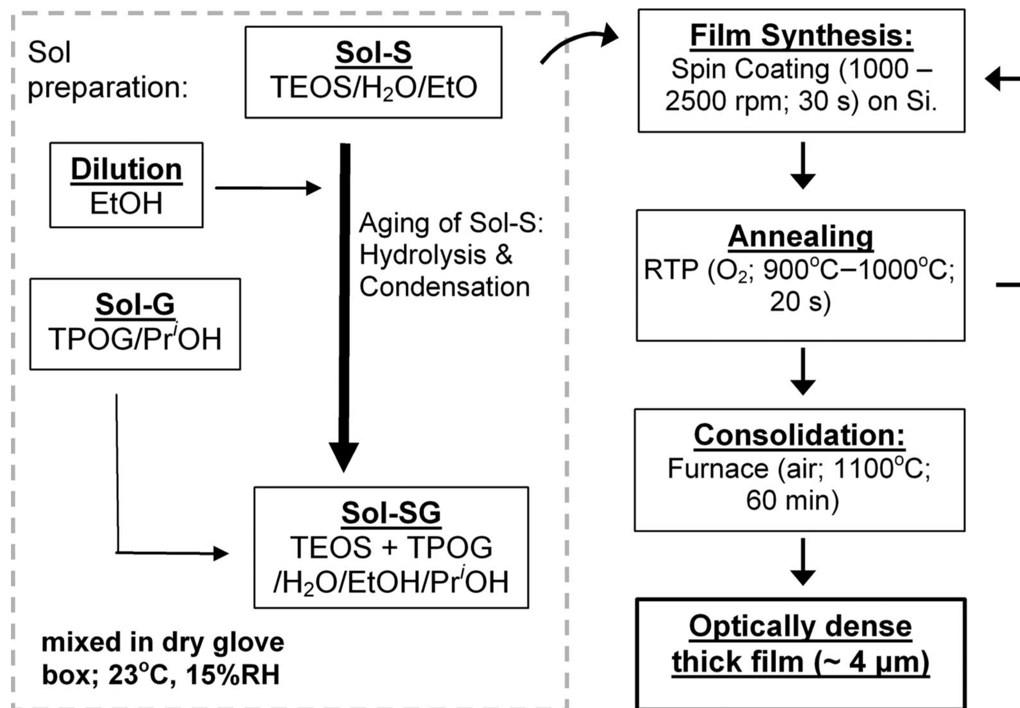

Fig. 1. Process flow of the fabrication of thick films involved in this work. The synthesis of porous or dense single-layer thin film essentially follows the same chemical mixing and spin coating procedures.

75° angles of incidence. The WVASE2.0 software was used to analyze the data from 210 to 1700 nm. The details of the measurements can be found in an earlier publication [11].

B. Ultraviolet-Imprinted Channel Waveguides

Multiple cycles of spin coating were required to achieve a suitable thickness of ~3 μm at a composition of $x \sim 0.20$ on a Si wafer with 10 μm thermal oxide. The RTP was used to anneal the sample at 900 °C in flowing O_2 gas after every coating cycle. A consolidation step was carried out in the electric furnace at 1000 °C for over 30 min. To form channel waveguides and devices by direct UV writing technique, the solgel-derived core germanosilicate layer was radiated using a KrF excimer laser (248 nm) for ~10 min at 450 mJ/pulse (beam size $24 \times 12\ \text{mm}^2$) and 10 Hz. The required RI contrast was realized by the use of a photomask in contact with the surface of the sample. Channel waveguides were characterized by taking a near-field image of the optical output by launching 1.55 μm lightwaves via a single-mode fiber (SMF) in a butt-couple configuration. The image was viewed with a 40× objective lens and recorded by a CCD camera using the BEAMProfile analysis software.

C. Solgel-Derived Encapsulant-Induced Quantum-Well Intermixing

The encapsulant porous GeO_2:SiO_2 was spin coated at 2500 rpm on substrates that contained the QWs. The lattice-matched InGaAs/InGaAsP QW laser structure was grown by metalorganic vapor phase epitaxy on (100)-oriented InP substrates as reported earlier [37]. The active region consists of five periods of 55 Å $In_{0.53}Ga_{0.47}As$ QWs with 120 Å InGaAsP barriers. Prior to the annealing using a RTP in flowing N_2 ambient for 2 min, the solgel capped samples were prebaked on a hot plate at 160 °C for 5 min to evaporate the residual solvent. QWI was activated by an annealing step at 630 °C for 2 min under flowing N_2 gas with a GaAs proximity cap. Photoluminescence (PL) at 77 K was performed on the QW samples to assess the degree of bandgap shift and linewidth broadening (viz., the extent of QWI) using an Nd:YAG laser (1.064 μm) as an excitation source.

3. Results and Discussions

A. Spectral Properties of Germanosilicate Films

To ensure an accurate reproduction of the optical constants from spectroscopic ellipsometry (SE) analysis, a rigorous characterization of the physical structure of the samples after annealing has been performed. In brief, the IR absorption spectra showed a high degree of random mixing between the germanium and silicon oxides and low OH content, and Rutherford backscattering (RBS) measurements revealed stoichiometric (i.e., O/(Ge + Si) = 2) binary oxide films were achieved [Fig. 2(a)]. Using the RUMP simulation, the areal atomic density of the film was determined from the RBS spectra. Combining with the thickness derived from the SE data, the density of the films was found. In Fig. 2(b) the density of the samples is in good agreement with the linear approximation calculated from the density of pure

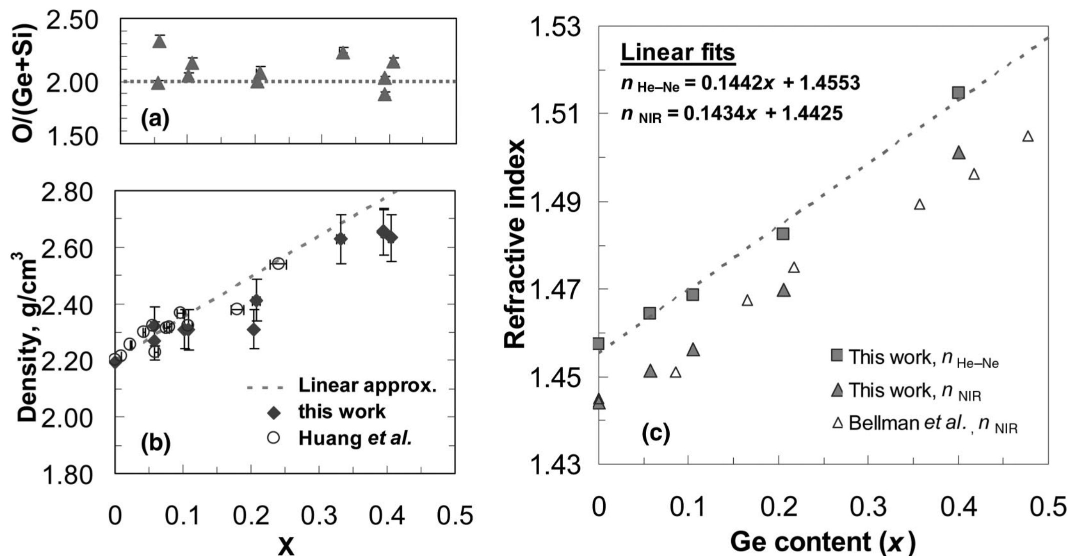

Fig. 2. (a) Stoichiometry of solgel synthesized xGeO$_2$:(1 − x)SiO$_2$ films determined by RBS. (b) Density of the films calculated using the areal atomic density from RBS and the thickness deduced from the SE analysis. (c) Linearity of the variation in RIs with composition. The dashed line represents the linear regression of the n(He–Ne) data from this work. RIs for the various important wavelengths are shown (see text).

SiO_2 and GeO_2 (i.e., 2.202 and 3.604 g/cm^3, respectively [7]) and the density values as determined by Huang *et al.* [7]. In an attempt to reduce the noise of the measurement data and to avoid possible correlation between the parameters of the dispersion model and others involved in the SE analysis, a multisample and multiangle measurement strategy was adopted [11,38,39] for a spectral range of 210–1700 nm.

Assuming negligible absorption (as validated by UV-VIS spectra down to 190 nm), the Sellmeier dispersion formula [38] was used to model the dispersion of the germanosilicate films. The Sellmeier dispersion formula is expressed as

$$n^2 = \varepsilon_0 + \frac{a\lambda^2}{\lambda^2 - b^2} - c\lambda^2, \quad (1)$$

where ε_0, a, b, c are the adjustable characteristic Sellmeier parameters. The SE model incorporating the Sellmeier dispersion formula shows good fits (mean-square error below 3) to the measured SE data. The resulting composition-dependent RI is clearly demonstrated in Fig. 2. Such a linear trend is typical of many silica-based materials [40], and the increase in RI with x as a result of an increase in polarizability and density can be explained by the Lorentz–Lorenz relationship [7,41]. A comparison with results from prior works at selected wavelengths illustrates the fidelity of the Sellmeier dispersion and that the density of the germanosilicate films fabricated using our solgel process is comparable to glasses formed by CVD [Bellman *et al.* [9], RI at 1550 nm, n(NIR)]. The Sellmeier dispersion relations representing the measured compositions are plotted in Fig. 3. The linear variation of RI with composition (x) noted in Fig. 2(c) allows an interpolation of the dispersion relationships forming a 3D data plot [11]. These data sets can then be used to predict values (either composition or RI) at a given wavelength.

In optical communications, the material dispersion coefficient, D_{MAT}, is defined as

$$D_{MAT} = -\frac{\lambda}{c}\frac{\partial^2 n}{\partial \lambda^2}, \quad (2)$$

where c refers to the speed of light in vacuum. The Sellmeier dispersion relationships determined from

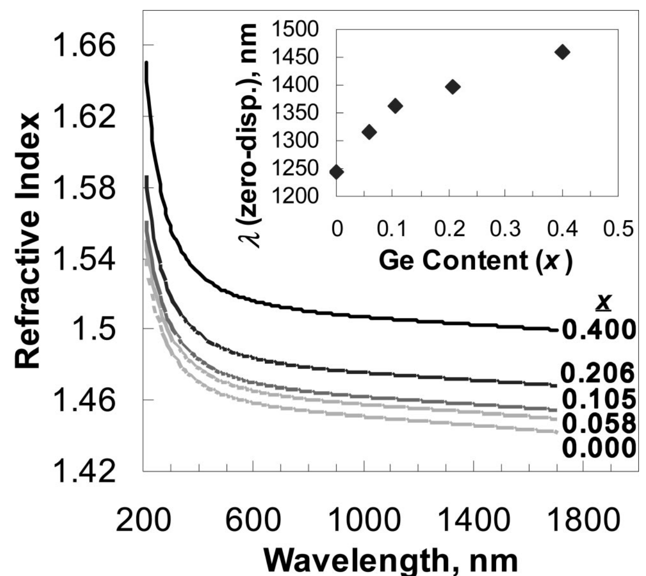

Fig. 3. Sellmeier dispersion for the selected compositions, $0 \leq x \leq 0.4$. Inset shows the zero-dispersion wavelengths for the different compositions.

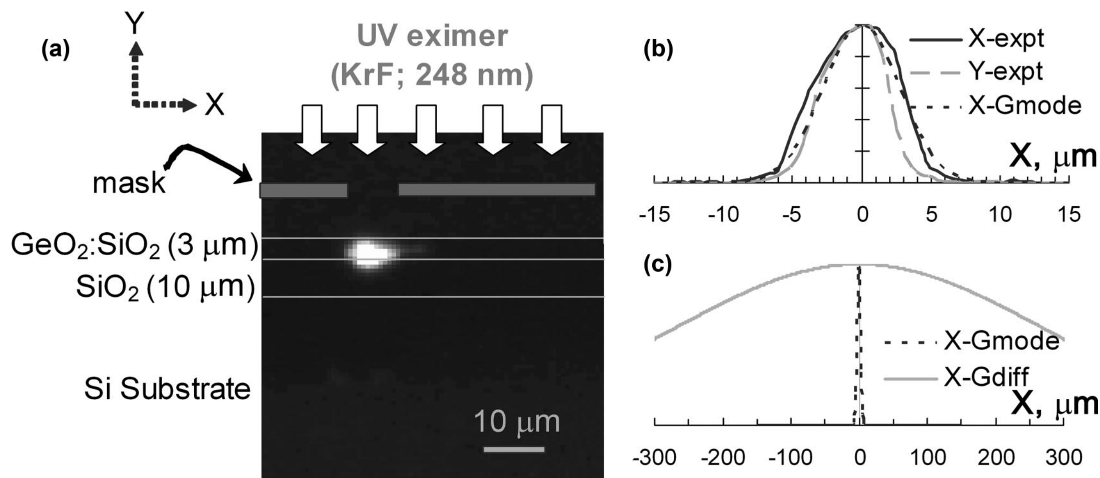

Fig. 4. (a) Near-field image of the optical output of a direct-written channel waveguide. Aperture of the mask is 5 μm. (b) Normalized intensity profiles of the measured beam profile across the X axis (X expt) and Y axis (Y expt); the theoretical profile derived from the Gaussian field approximation (X-Gmode); the abscissa is in units of micrometers. (c) Comparison between the Gaussian approximation of intensity profile with guiding (X Gmode) and without guiding (X Gdiff) in X.

the SE analysis can be used to calculate D_{MAT} for each composition (x) by substituting Eq. (1) into Eq. (2). Setting $D_{MAT} = 0$, the zero-dispersion wavelength is shown to increase with x (inset of Fig. 3). We then conclude that the material dispersion is sensitive to the Ge content within the optical communication window, and the zero-dispersion wavelength can be tailored by selecting a specific x value.

B. Photosensitivity and Direct Writing of Optical Waveguides

Although laser-written waveguides in SiO_2 have been reported [42], the incorporation of GeO_2 will enhance the achievable increase in the change of an UV-induced RI, Δn [23]. A Δn of 2.3×10^{-3} was achieved in a planar waveguide (core-layer thickness of ~3 μm) with low loss <0.5 dB/cm as characterized by the prism-coupled configuration [27]. A single-mode optical signal can be seen quite clearly from the figure for a 6 mm long channel waveguide Fig. 4(a).

The effectiveness of the optical guiding ability can be seen through the intensity profiles of the near-field image. The measured profiles along the X and Y axes are shown respectively as X expt and Y expt in Fig. 4(b). A profile of a Gaussian approximation of the fundamental mode, using the value of Δn as measured by the prism coupler, is presented (X Gmode) as a comparison. The asymmetry of the Y expt profile can be understood from the inherent air-GeO:SiO_2-SiO_2 structure. The slight asymmetry of the X expt curve could possibly be attributable to the imperfections in the UV irradiation setup leading to nonuniform irradiance and/or nonpolished end face of the waveguide, causing wavefront distortion at the waveguide output. Without guiding (i.e., planar waveguide without UV exposure), the lightwaves launched from the SMF after a propagation length of 500 μm in the waveguide would experience diffraction, causing broadening of the beam profile as shown by X Gdiff in Fig. 4(c) along the X axis. The theoretical intensity profiles were calculated according to expressions given in a prior report [43]. From the comparison of X expt, X Gmode, and X Gdiff, the achieved Δn and effectiveness of the direct-writing technique can be ascertained. This is made possible owing to the ability to induce relatively high Δn by the UV radiation to confine the lightwaves. In most cases, the values of Δn are relatively small, of the order of 10^{-5}–10^{-4} [44,45], which are inadequate for strong confinement of the lightwaves. The change in refractive index is normally explained in terms of a number of photochemical reactions involving oxygen-deficient defects such as the neutral oxygen monovacancy (NOMV) and Ge^{2+} [44,45]. The defects are shown schematically in Fig. 5.

Sakoh *et al.* [26] reported a RI change of approximately 10^{-3} involving highly photosensitive Ge^{2+} centers [(Fig. 5(c)]. Our work has shown that Δn of as high as 9.8×10^{-3} for films of thickness ~200 nm can be achieved by the combination of UV radiation and the solgel spin-coating process, yielding pure inorganic films [27]. This relatively high value of Δn is explained in terms of the creation of oxygen related defects [27].

C. Quantum-Well Intermixing Using Germanosilicate Encapsulant Layer

The annealed bare sample of an incomplete laser structure used in this study, shown in Fig. 6(a), exhibits only a small bandgap blueshift of ~12 nm. The incomplete structure refers to the full laser structure after subsequent removal of highly doped InGaAs contact layers above the QW region. Figure 6(a) also shows that a change in the PL peak wavelength is affected by the compositions of the germanosilicate cap layer. Evidently, the solgel cap enhances the intermixing rate in QWs. At Ge content of $x < 0.1$, the

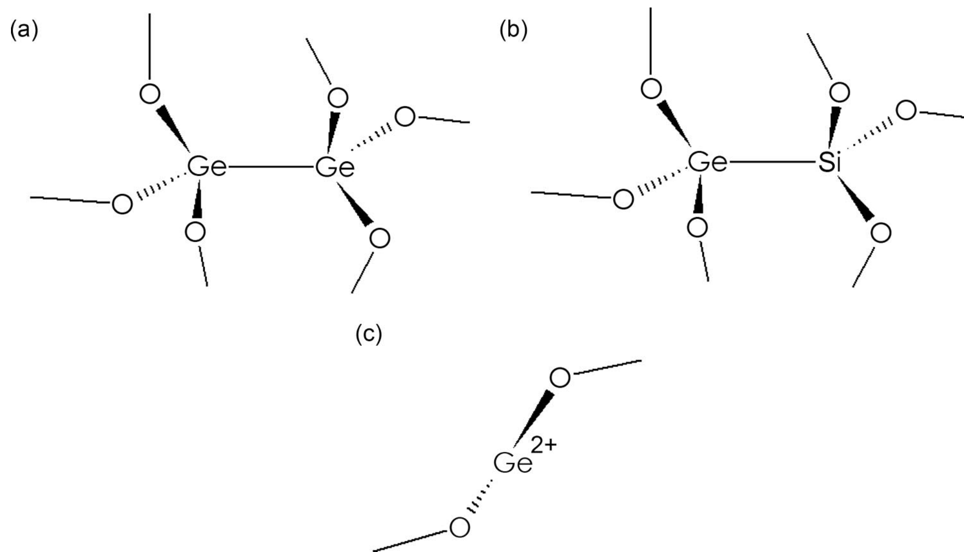

Fig. 5. Oxygen-deficient defects commonly found in GeO_2 and GeO_2:SiO_2 glasses. Defects (a) and (b) are known as NOMV and can be identified by an absorption band ~5.1 eV. Defect (c) consists of a divalent Ge, which is known to absorb 5.16 eV.

PL peak shift remains constant at ~16 nm. Beyond this there is nearly a linear increase in the PL shift up to $x \sim 0.30$.

We further perform the intermixing study on the complete QW laser structure to demonstrate the post-growth bandgap tuning using the solgel cap. Bare (uncapped) samples and samples capped by *e*-beam-evaporated SiO_2 (EBSi) were also annealed for comparison. In Fig. 6(b), we obtain four distinguished PL spectra from bare samples and capped samples with the EBSi and Ge-doped solgels ($x = 0.00$ and 0.16). The PL peaks for EBSi, uncapped, $x = 0$ and 0.16 are respectively 1456, 1436, 1408, and 1392 nm. This result highlights the spatial bandgap selectivity using a combination of dielectric caps. The control sample and the intermixed sample ($x = 0.16$) exhibit a comparable PL linewidth (~40 meV) while the as-grown PL has a linewidth of 44 meV. The negligibly small linewidth broadening infers the retention of the optical quality after intermixing. The overall blueshifts in the complete laser structure are enhanced when compared to the incomplete structure. The presence of Ga atoms from the InGaAs contact layer below the solgel cap is responsible for the increase in the degree of intermixing from the complete laser structure.

It has been known that porosity and thermal expansion of the cap are two important parameters for the dielectric layer in dielectric cap-induced disordering [33]. From the curves of (iii) and (iv), the solgel caps exhibit an enhancement in the degree of inter-

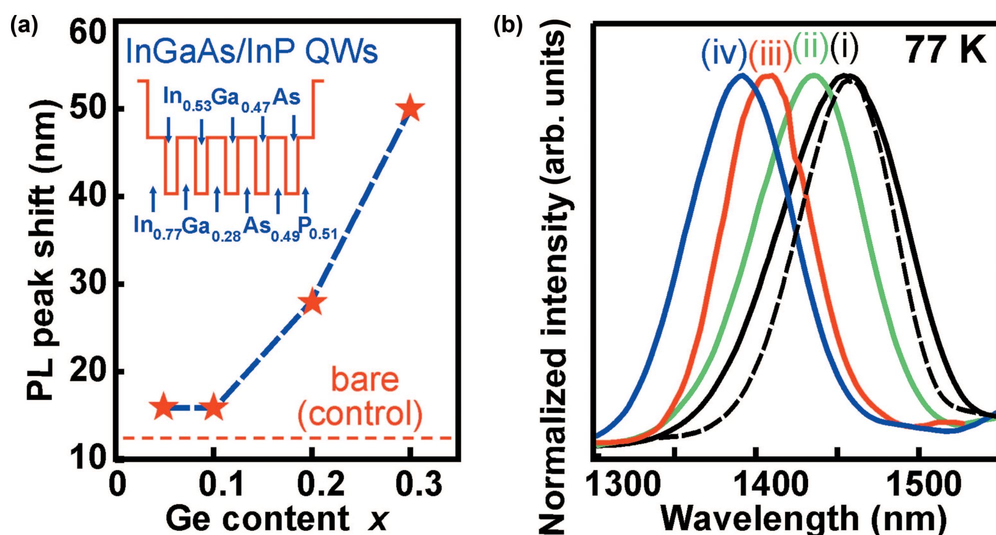

Fig. 6. (Color online) (a) Effect of Ge content (x) of the solgel cap on the PL peak wavelength shift of the QW partial laser structure. The dashed line represents the amount of bandgap shift observed from the annealed bare samples as a control. The inset is the InGaAs/InGaAsP multiple QWs used in the experiment. (b) PL spectra at annealing temperature of 630 °C from (i) *e*-beam evaporated SiO_2 capped, (ii) bare, (iii) $x = 0.00$, (iv) $x \sim 0.16$ capped QWs. The dashed curve represents the as-grown PI.

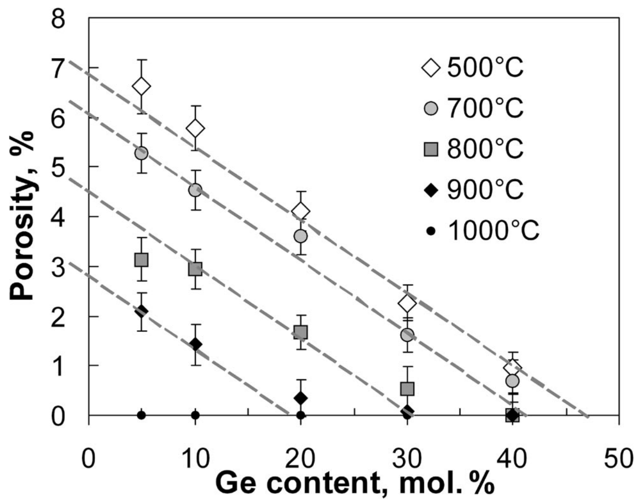

Fig. 7. Porosity–Ge map demonstrating both the effect of annealing temperature and Ge content on the film porosity; dashed lines represent a fit-by-eye guide for the data points at each annealing temperature [47].

mixing when compared to the EBSi film due to the porous nature as observed earlier in our FTIR and ellipsometry results [46]. Figure 7 summarizes the relationship of porosity and the Ge content in the solgel films with the annealing treatments. The incorporation of Ge into the films gives a reduction in the porosity of films. This contradicts the intermixing enhancement results in the $x \sim 0.16$ caps if the porosity is the dominant effect in the solgel cap-induced intermixing. We identify that there is a substantial increase in the thermal expansion with the addition of Ge into the films [7]. Compressive stress is known to favor the transformation of vacancy defects into antisites [33,47], hence the degree of intermixing is reduced. Such compressive stress in the semiconductor QWs exists because of the large difference in the coefficients of the semiconductor material ($\sim 10^{-6}$) and the solgel glass ($\sim 10^{-7}$). Considering the magnitude of change in the cap porosity and the thermal expansion as a result of the increase in Ge content, an estimate can be obtained from the above references to be $[(4.4\% - 6.8\%)/6.8\% \times 100] \sim -35.3\%$ (see Fig. 7) and $[(2.4 - 0.5)/0.5 \times 100] \sim 380\%$ [7], respectively. Although the relative effect of the above two parameters for the current material system is not known, the change in the thermal expansion is likely to be the dominating factor that enables the control of the QWI via vacancy diffusion by the addition of Ge.

To further substantiate the vacancy outdiffusion role in the QWI enhancement at various Ge content, we carried out a similar intermixing process to the GaAs/AlGaAs multiwidth QWs structure. The structure was chosen for two main reasons. First, the intermixing in this structure is solely governed by the group III atomic interdiffusion from the effective Ga vacancy injection. Second, the structure permits the depth-resolved intermixing degree by measuring the change in the individual PL peak after intermixing [48]. We compare the GaAs/AlGaAs QW intermixing with $x = 0.10$ and $x = 0.40$ at relatively low annealing temperatures for GaAs-based QWI in Fig. 8. Note that the typical QWI process temperature for the GaAs/AlGaAs system is above 850 °C. At this annealing condition, there is no effect on the thermal shift under control samples. Figure 8(a) shows the insignificant QWI effect in the $x \sim 0.1$ cap at RTA of 650 °C, which is similar to the previous case in the InGaAsP QWs. In ths case of $x \sim 0.4$ cap, the QWI effect is greatly pronounced, and the PL spectra has been blueshifted for all four QWs. The signal corresponding to the narrowest well, QWI, is not clearly resolved after annealing, implying that the well has

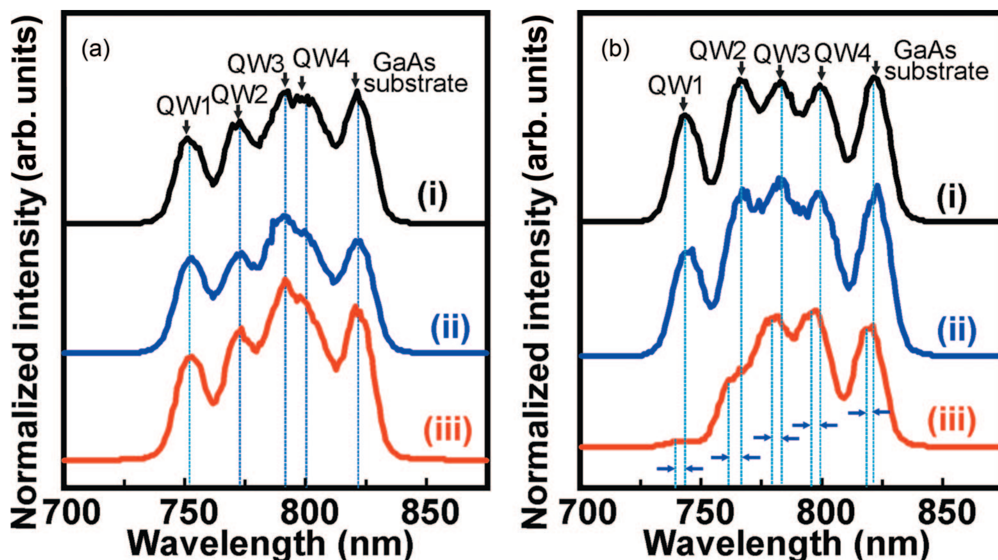

Fig. 8. (Color online) Photoluminescence at 77 K from (i) as-grown, (ii) control (annealed bare), and (iii) solgel capped samples: with (a) $x = 0.1$ and (b) $x = 0.40$ to the intermixing in the $GaAs/Al_{0.2}Ga_{0.8}As$ multiwidth QWs (QW1, 3 nm; QW2, 5 nm; QW3, 6 nm; and QW4, 8 nm). The annealing was performed at 650 °C for 2 min.

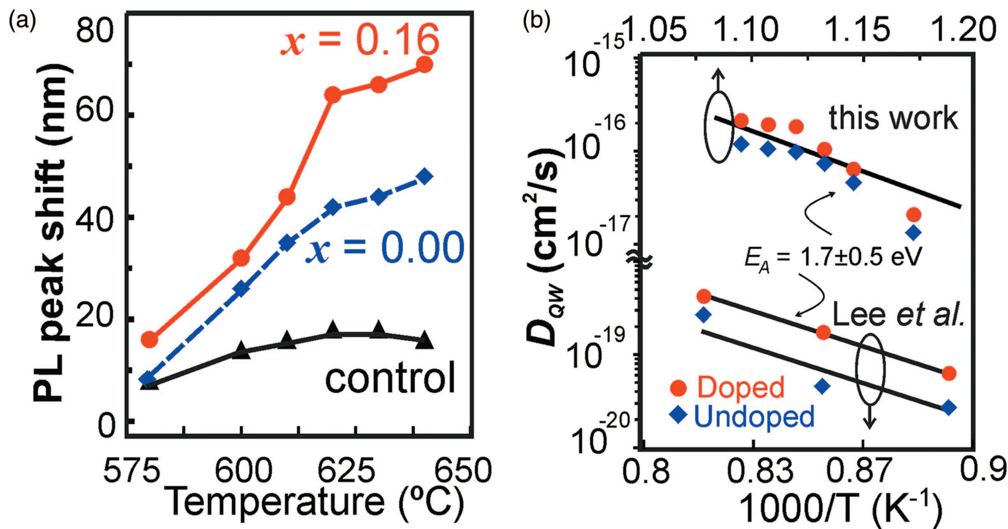

Fig. 9. (Color online) (a) PL peak wavelength shift versus the annealing temperature of an InGaAs/InP QW laser structure. (b) Diffusion coefficient of QW (D_{QW}) deduced from the experimental data as a function of the inversed annealing temperature for doped and undoped solgel caps in our present work (InP substrate) and Lee *et al.* [51] (GaAs substrate). A representative best linear fit is shown for both data sets, whose slopes correspond to the activation energy.

been totally intermixed or dissolved to the surrounding AlGaAs barrier. The result further validates the role of efficient creation of beneficial vacancies via stress relaxation in the Ge-added solgel that leads to the pronounced degree of intermixing.

The activation energy and diffusion coefficient correspond to the energy associated with the motion and formation of defects during the dielectric cap annealing process. The annealing temperature-dependent bandgap shift can be used to deduce the diffusion coefficients (assumed to be independent of defect concentration), D_{QW}, and to extract the activation energy, E_A [49]. Figure 9(a) summarizes the relationship of annealing temperature and bandgap shift for caps of $x = 0.00$ and 0.16 from the InGaAs-InP QWs using Ge-dopant. For completion, we also include the experimental data of solgel cap-induced intermixing on GaAs substrate by Lee *et al.* [50]. As shown in Figure 9(b), the experimental data are linearly fitted over $1000/T$ to the Arrhenius equation $D_{QW} \sim \exp(-E_A/kT)$, where T and E_A refer to the annealing temperature and the activation energy, respectively. This yields the extracted $E_A = 1.7 \pm 0.5$ eV for both cases, which is significantly lower than the common InP-based and GaAs-based QWI processes [51,52]. Nearly identical E_A intuitively implies that the discrepancy in interdiffusion behavior between $x \sim 0.16$ and $x = 0.00$ is only attributed to the difference in the number of beneficial vacancies that involve in the QWI, which is in good agreement with the experimental data of the GaAs/AlGaAs QW intermixing earlier. This result further corroborates postulation that the compressive stress reduces the effective vacancy responsible for intermixing enhancement in the Ge-added film. Therefore the enhancement of QWI by the increased doping of the Ge content can be ascribed to the large magnitude of change in the thermal expansion leading to the retention of vacancies that drives QWI.

Understanding that stress, rather than porosity, has a dominant affect in the QWI in the above scheme, some inferences can be made about the selection of the suitable process that takes advantage of the QWI control using the GeO_2:SiO_2 solgel caps in implementing spatial-selective QWI on semiconductor platforms. Pepin *et al.* [31] and Deenapanray *et al.* [53] have shown that by depositing a Si_3N_4 layer atop of a patterned or nonpatterned encapsulant SiO_2 layer, QWI was univocally suppressed while a single layer SiO_2 typically enhances QWI. This unexpected observation was attributed to the fact that the near-surface stress distribution in the semiconductor was drastically modified (i.e., reversed). Therefore the QWI performance of spatial areas, which are underneath any multiple layer of varying GeO_2:SiO_2 solgel films may deviate from the results found in the present work. On the contrary, if the cap porosity was the more dominant factor in the QWI process, then the above stress-induced QWI deviation is unlikely to occur. As a foresight, there are a number of low-cost processes that are well suited to implement the above QWI scheme. Such process as printing, which involves the simultaneous deposition of multiple solutions, may open up new opportunities for low-cost photonic integration.

4. Conclusion

Optical constants have been modeled by the Sellmeier dispersion for films with compositions of $x \leq 0.400$ over a broad spectral range of 210 to 1700 nm. The RI-composition-wavelength 3D dataset enables self-consistent prediction of values with two known parameter values. Further work is ongoing in an attempt to parameterize the Sellmeier values with

the composition of the germanosilicate films. Theoretically, pure GeO_2 is a better candidate than germanosilicate for the various applications in planar lightwave circuits and direct writing. However, germanosilicate ($x \geq 0.600$) or GeO_2 is known to be hygroscopic, and special chemical treatment is required for handling the solgel chemistry with a high content of germanium precursors. Thus work involving germanosilicate of $x > 0.40$ is beyond the scope of this article. Motivated by the possibility of the UV imprinting of waveguide devices (with appreciable RI contrast, Δn) and the commercial attractiveness of the solgel process, work has been done to improve the quality (uniformity and spin-coating artifacts) of germanosilicate films in the view of complex large-area devices and large-scale integration. Results will be reported elsewhere. Besides the low-cost aspects of the solgel process, the unique and adjustable properties of solgel derived films of germanosilicate glass (viz., porosity and thermal expansion) afford tunability of the bandgap energy in QW structures via QWI for III–V platforms (such as InGaAs(P)/InP) that have inherently low thermal stability.

This work was funded in part by the Agency for Science, Technology and Research (A*STAR) in Singapore under the Optical Networking Focused Interests Group (ONFIG) project. C. K. F. Ho and Rajni acknowledge the Research Scholarship provided by Nanyang Technological University.

References

1. K. O. Hill and G. Meltz, "Fiber Bragg grating technology fundamentals and overview," J. Lightwave Technol. **15,** 1263–1276 (1997).
2. Rajni, K. Pita, S. F. Yu, S. C. Tjin, and C. H. Kam, "Fabrication of inorganic GeO_2:SiO_2 channel waveguides by ultraviolet imprinting technique," Appl. Phys. Lett. **89,** 071105 (2006).
3. R. R. A. Syms and J. R. Cozens, *Optical Guided Waves and Devices* (McGraw-Hill, 1992).
4. F. Ladouceur and J. D. Love, *Silica-Based Buried Channel Waveguides and Devices,* Optical and Quantum Electronics Series (Chapman & Hall, 1996).
5. C. R. Pollock and M. Lipson, *Integrated Photonics* (Kluwer Academic, 2003).
6. K. Susa, I. Matsuyama, S. Satoh, and T. Suganuma, "Sol-gel derived Ge-doped silica glass for optical fiber application. I. Preparation of gel and glass and their characterization," J. Non-Cryst. Solids **119,** 21–28 (1990).
7. Y. Y. Huang, A. Sarkar, and P. C. Schultz, "Relationship between composition, density and refractive index for germania silica glasses," J. Non-Cryst. Solids **27,** 29–37 (1978).
8. D.-G. Chen, B. G. Potter, and J. H. Simmons, "GeO_2-SiO_2 thin films for planar waveguide applications," J. Non-Cryst. Solids **178,** 135–147 (1994).
9. R. A. Bellman, G. Bourdon, G. Alibert, A. Beguin, E. Guiot, L. B. Simpson, P. Lehuede, L. Guiziou, and E. LeGuen, "Ultralow loss high delta silica germania planar waveguides," J. Electrochem. Soc. **151,** G541–G547 (2004).
10. A. B. Djurisic, Y. Chan, and E. H. Li, "Progress in the room-temperature optical functions of semiconductors," Mater. Sci. Eng., R. **38,** 237–293 (2002).
11. C. K. F. Ho, K. Pita, N. Q. Ngo, and C. H. Kam, "Optical functions of $(x)GeO_2$:$(1-x)SiO_2$ films determined by multi-sample and multiangle spectroscopic ellipsometry," Opt. Express **13,** 1049–1054 (2005).
12. M. Abe, K. Takada, T. Tanaka, M. Itoh, T. Kitoh, and Y. Hibino, "Reduction in dispersion of silica-based AWG using photosensitive phase trimming technique," Electron. Lett. **38,** 1673–1675 (2002).
13. J. Gehler and F. Knappe, "Crosstalk reduction of arrayed waveguide gratings by UV trimming of individual waveguides without H_2-loading," in *Optical Fiber Communication Conference,* Vol. 37 of OSA Trends in Optics and Photonics Series (Optical Society of America, 2000), paper WM9.
14. K. Takada and M. Abe, "UV trimming of AWG devices," in *Bragg Gratings Photosensitivity and Poling in Glass Waveguides,* Vol. 93 in OSA Trends in Optics and Photonics Series (Optical Society of America, 2003), pp. 175–177.
15. D. A. Zauner, J. Hubner, K. J. Malone, and M. Kristensen, "UV trimming of arrayed-waveguide grating wavelength division demultiplexers," Electron. Lett. **34,** 780–781 (1998).
16. Q. Y. Zhang, K. Pita, C. K. F. Ho, N. Q. Ngo, L. P. Zuo, and S. Takahashi, "Low optical loss germanosilicate planar waveguides by low-pressure inductively coupled plasma-enhanced chemical vapor deposition," Chem. Phys. Lett. **368,** 183–188 (2003).
17. M. Takahashi, A. Sakoh, Y. Tokuda, T. Yoko, J. Nishii, H. Nishiyama, and I. Miyamoto, "Photochemical process of divalent germanium responsible for photorefractive index change in GeO_2-SiO_2 glasses," J. Non-Cryst. Solids **345–346,** 323–327 (2004).
18. M. Takahashi, K. Ichii, Y. Tokuda, T. Uchino, T. Yoko, J. Nishii, and T. Fujiwara, "Photochemical reaction of divalent-germanium center in germanosilicate glasses under intense near-ultraviolet laser excitation: Origin of 5.7 eV band and site selective excitation of divalent-germanium center," J. Appl. Phys. **92,** 3442–3446 (2002).
19. J. Nishii, "Permanent index changes in Ge-SiO_2 glasses by excimer laser irradiation," Mater. Sci. Eng. B **54,** 1–10 (1998).
20. S. Agnello, R. Boscaino, F. La Mattina, S. Grandi, and A. Magistris, "Hydrogen-related paramagnetic centers in Ge-doped sol-gel silica induced by γ-ray irradiation," J. Sol-Gel Sci. Technol. **37,** 63–68 (2006).
21. J. Nishii, H. Yamanaka, H. Hosono, and H. Kawazoe, "Characteristics of 5-eV absorption band in sputter deposited GeO_2-SiO_2 thin glass films," Appl. Phys. Lett. **64,** 282–284 (1994).
22. H. Hosono, Y. Abe, D. L. Kinser, R. A. Weeks, K. Muta, and H. Kawazoe, "Nature and origin of the 5-eV band in GeO_2:SiO_2 glasses," Phys. Rev. B **46,** 11445–11451 (1992).
23. K. D. Simmons, G. I. Stegeman, B. G. Potter, Jr., and J. H. Simmons, "Photosensitivity in germano-silicate sol-gel thin films," J. Non-Cryst. Solids **179,** 254–259 (1994).
24. M. Fokine and W. Margulis, "Large increase in photosensitivity through massive hydroxyl formation," Opt. Lett. **25,** 302–304 (2000).
25. M. G. Sceats, G. R. Atkins, and S. B. Poole, "Photolytic index changes in optical fibers," Annu. Rev. Mater. Sci. **23,** 381–410 (1993).
26. A. Sakoh, M. Takahashi, T. Yoko, J. Nishii, H. Nishiyama, and I. Miyamoto, "Photochemical process of divalent germanium responsible for photorefractive index change in GeO_2-SiO_2 glasses," Opt. Express **11,** 2679–2688 (2003).
27. Rajni, K. Pita, S. C. Tjin, S. F. Yu, and C. H. Kam, "Enhanced photosensitivity in sol-gel derived $20GeO_2$:$80SiO_2$ thin films," Appl. Phys. A **82,** 535–541 (2006).
28. J. H. Marsh, "Quantum well intermixing," Semicond. Sci. Technol. **8,** 1136–1155 (1993).
29. E. H. Li, ed., *Semiconductor Quantum Wells Intermixing,* Optoelectronic Properties of Semiconductors and Superlattices, Vol. 8 (Gordon & Breach, 2000), p. 695.
30. A. M. Kan'an, P. LiKamWa, Mitra-Dutta, and J. Pamulapati,

"Area-selective disordering of multiple quantum well structures and its applications to all-optical devices," J. Appl. Phys. **80,** 3179–3183 (1996).
31. A. Pepin, C. Vieu, M. Schneider, H. Launois, and Y. Nissim, "Evidence of stress dependence in SiO_2/Si_3N_4 encapsulation-based layer disordering of GaAs/AlGaAs quantum well heterostructures," J. Vac. Sci. Technol. B **15,** 142–153 (1997).
32. P. Cusumano, B. S. Ooi, A. S. Helmy, S. G. Ayling, A. C. Bryce, J. H. Marsh, B. Voegele, and M. J. Rose, "Suppression of quantum well intermixing in GaAs/AlGaAs laser structures using phosphorus-doped SiO_2 encapsulant layer," J. Appl. Phys. **81,** 2445–2447 (1997).
33. P. N. K. Deenapanray, B. Gong, R. N. Lamb, A. Martin, L. Fu, H. H. Tan, and C. Jagadish, "Impurity-free disordering mechanisms in GaAs-based structures using doped spin-on silica layers," Appl. Phys. Lett. **80,** 4351–4353 (2002).
34. H. S. Djie, C. K. F. Ho, T. Mei, and B. S. Ooi, "Quantum well intermixing enhancement using Ge-doped sol-gel derived SiO_2 encapsulant layer in InGaAs/InP laser structure," Appl. Phys. Lett. **86,** 081106 (2005).
35. R. R. A. Syms, "Stress in thick sol-gel phosphosilicate glass films formed on Si substrates," J. Non-Cryst. Solids **167,** 16–20 (1994).
36. R. R. A. Syms and A. S. Holmes, "Deposition of thick silica-titania sol-gel films on Si substrates," J. Non-Cryst. Solids **170,** 223–233 (1994).
37. H. S. Lim, V. Aimez, B. S. Ooi, J. Beauvais, and J. Beerens, "A novel fabrication technique for multiple-wavelength photonic-integrated devices in InGaAs-InGaAsP laser heterostructures," Photon. Technol. Lett. **14,** 594–596 (2002).
38. C. M. Herzinger, B. Johs, W. A. McGahan, J. A. Woollam, and W. Paulson, "Ellipsometric determination of optical constants for silicon and thermally grown silicon dioxide via a multi-sample, multiwavelength, multiangle investigation," J. Appl. Phys. **83,** 3323–3336 (1998).
39. C. M. Herzinger, B. Johs, W. A. McGahan, and W. Paulson, "A multisample, multiwavelength, multiangle investigation of the interface layer between silicon and thermally grown silicon dioxide," Thin Solid Films **313,** 281–285 (1998).
40. H. Scholze, *Glass: Nature, Structure, and Properties* (Springer-Verlag, 1991).
41. M. Born and E. Wolf, *Principles of Optics,* 2nd ed. (Pergamon Press, 1964).
42. T. Pertsch, U. Peschel, F. Lederer, J. Burghoff, M. Will, S. Nolte, and A. Tunnermann, "Discrete diffraction in two-dimensional arrays of coupled waveguides in silica," Opt. Lett. **29,** 468–470 (2004).
43. J. Zhou, N. Q. Ngo, K. Pita, C. H. Kam, P. V. Ramana, and M. K. Iyer, "Determining the minimum number of arrayed waveguides and the optimal orientation angle of slab for the design of arrayed waveguide gratings," Opt. Commun. **226,** 181–189 (2003).
44. Q. Y. Zhang, K. Pita, S. C. Tjin, C. H. Kam, L. P. Zuo, and S. Takahashi, "Laser-induced ultraviolet absorption and refractive index changes in Ge-B-SiO_2 planar waveguides by inductively coupled plasma-enhanced chemical vapor deposition," Chem. Phys. Lett. **379,** 534–538 (2003).
45. M. Essid, J. Albert, J. L. Brebner, and K. Awazu, "Correlation between oxygen-deficient center concentration and KrF excimer laser induced defects in thermally annealed Ge-doped optical fiber preforms," J. Non-Cryst. Solids **246,** 39–45 (1999).
46. C. K. F. Ho, H. S. Djie, K. Pita, N. Q. Ngo, and C. H. Kam, "Sintering and porosity control of $(x)GeO_2:(1-x)SiO_2$ sol-gel derived films for optoelectronic applications," Electrochem. Solid-State Lett. **7,** 96–98 (2004).
47. S. Doshi, P. N. K. Deenapanray, H. H. Tan, and C. Jagadish, "Towards a better understanding of the operative mechanisms underlying impurity-free disordering of GaAs: Effect of stress," J. Vac. Sci. Technol. B **21,** 198–203 (2003).
48. H. S. Djie, T. Mei, J. Arokiaraj, and D. Nie, "Single step quantum well intermixing with multiple band gap control for III-V compound semiconductors," J. Appl. Phys. **96,** 3282–3285 (2004).
49. H. S. Djie, S. L. Ng, O. Gunawan, P. Dowd, V. Aimez, J. Beauvais, and J. Beerens, "Analysis of strain-induced polarisation-insensitive integrated waveguides fabricated using ion-implantation-induced intermixing," IEE Proc. Optoelectron. **149,** 138–144 (2002).
50. L. H. Lee, B. S. Ooi, Y. Lam, Y. C. Chan, and C. H. Kam, "Quantum well intermixing in GaAs-AlGaAs laser structure using sol-gel SiO_2 dielectric cap," Proc. SPIE **3547,** 319–323 (1998).
51. S. S. Rao, W. P. Gillin, and K. P. Homewood, "Interdiffusion of the group-III sublattice in In-Ga-As-P/In-Ga-As-P and In-Ga-As/In-Ga-As heterostructures," Phys. Rev. B **50,** 8071–8073 (1994).
52. O. M. Khreis, W. P. Gillin, and K. P. Homewood, "Interdiffusion: a probe of vacancy diffusion in III-V materials," Phys. Rev. B **55,** 15813–15818 (1997).
53. P. N. K. Deenapanray, A. Martin, and C. Jagadish, "Defect engineering in annealed n-type GaAs epilayers using SiO_2/Si_3N_4 stacking layers," Appl. Phys. Lett. **79,** 2561–2563 (2001).